On Presolar Grains from CO Classical Novae

Christian Iliadis

Department of Physics & Astronomy, University of North Carolina, Chapel Hill, NC 27599-3255
Triangle Universities Nuclear Laboratory, Durham, NC 27708-0308, USA

iliadis@unc.edu

Lori N. Downen

Department of Physics & Astronomy, University of North Carolina, Chapel Hill, NC 27599-3255
Triangle Universities Nuclear Laboratory, Durham, NC 27708-0308, USA

Jordi José

Departament de Física, EEBE, Universitat Politècnica de Catalunya, c/Eduard Maristany 10, E-08930 Barcelona, Spain
Institut d'Estudis Espacials de Catalunya, c/Gran Capità 2-4, Ed. Nexus-201, E-08034 Barcelona, Spain

Larry R. Nittler

Department of Terrestrial Magnetism, Carnegie Institution for Science, Washington, DC 20015, USA

Sumner Starrfield

Department of Physics and Astronomy, Arizona State University, Tempe, AZ 85287-1504, USA

ABSTRACT

xxx.

Subject headings: stars: abundances — xxx

1. Introduction

Primitive meteorites contain dust grains of isotopic composition vastly different compared to any other matter found in the solar system (Zinner 2014). The only viable explanation for their existence is that they condensed in stellar winds or the ejecta of exploding stars. These tiny grains survived the journey through the interstellar medium to the region in which the presolar cloud formed about 4.6 Gy ago. Some of these grains also survived the homogenization process during the formation of the solar system and were incorporated into meteorites. They are called presolar grains, or stardust, and they retain the distinct isotopic composition of the stellar outflows at the time of grain condensation. The laboratory measurement of their isotopic ratios provides an exceptional opportunity to study stellar evolution, stellar explosions, nucleosynthesis, dust formation, and galactic chemical evolution.

The analysis and interpretation of presolar grains require an iterative approach (Nittler & Cielsa 2016). First, the stellar source for a group of grains needs to be identified on the basis of the available isotopic data. Once the source is identifed, the precisely measured isotopic ratios provide strong constraints for understanding the physical and chemical processes that occurred inside the parent stars. According to current thinking, most analyzed presolar grains have formed in Asymptotic Giant Branch (AGB) stars of a previous generation. This insight was important for a quantitative understanding of AGB stars, and also for demonstrating how one half of all elements beyond iron are synthesized in the astrophysical s-process. A fraction of the measured presolar grains originate presumably from core-collapse supernovae **(Jordi - please quantify and provide references)**. Their isotopic signatures may shed light on explosive nucleosynthesis, the mixing between different layers in the ejecta, grain condensation, and how much dust survives the reverse shock before injection into the interstellar medium.

A few presolar grains are characterized by very low ^{12}C/^{13}C and ^{14}N/^{15}N ratios and large ^{30}Si excesses (Amari et al. 2001). These signatures imply an increased production of the minor isotopes, ^{13}C and ^{15}N, compared to the major ones, ^{12}C and ^{14}N, and are difficult to explain by AGB star or supernova nucleosynthesis. Explosive hydrogen burning in classical novae, on the other hand, seems to reproduce qualitatively some of the isotopic signatures measured in these grains (Amari et al. 2001; José et al. 2004; José & Hernanz 2007; Haenecour et al. 2016).

A classical nova is thought to be one consequence of the accretion of hydrogen-rich material onto a white dwarf in a close binary system (José et al. 2016; Starrfield, Iliadis, & Hix 2016). Some of the key processes are sketched in Figure 1. Over long periods of time, the material being accreted from the secondary star forms a layer of nuclear fuel (green region in Figure 1a) on the white dwarf surface. The bottom of this layer is gradually compressed by the surface gravity and becomes electron degenerate. Once the temperature at the bottom of the accreted layer reaches the Fermi temperature ($\approx$ 30 MK), the layer begins to expand, but by this time the temperature is increasing so fast that a thermonuclear runaway results. During the steep temperature rise, matter from the outermost white dwarf core layer is dredged up into the accreted matter (red region in Figure 1b), as first suggested by Ferland & Shields (1978). This significantly enriches the burning layer in CNO nuclei, which is crucial for ensuring a strong nuclear energy release and a violent outburst; it also helps explaining the observed abundances inferred from the ejecta. The ejected material (green region in Figure 1c) consists of a mixture of white dwarf and accreted matter that has been processed by explosive hydrogen burning.

Spectroscopic studies identified two distinct types of classical novae. Nova shells rich in CNO material point to an underlying CO white dwarf, which represents the evolutionary fate of a low-mass star after the cessation of core helium burning. These objects are also called "CO novae". On the other hand, element enrichments in the range from Ne to Ar have been attributed to the presence of an underlying, massive ONe white dwarf, representing the evolutionary fate of an intermediate-mass star after completion of core carbon burning. The latter explosions, often referred to as "neon novae" or "ONe novae", tend to be much more energetic than CO novae (Starrfield, Sparks, & Truran 1986).

About 20-100 days after the outburst,

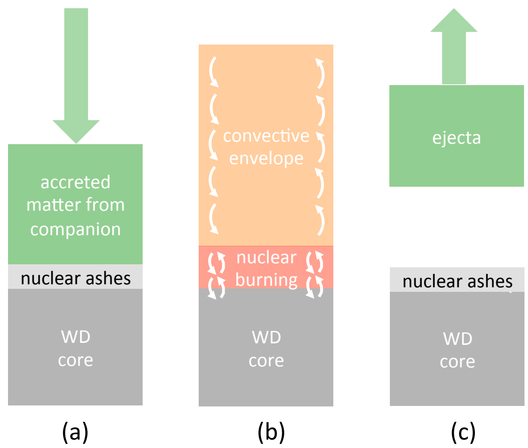

Fig. 1.— Sketch of processes during a classical nova outburst. (a) Nuclear ashes from a previous outburst (H, He; light grey region) sit on top of a CO-rich white dwarf core (dark grey region), consisting mainly of ^{12}C and ^{16}O; the white dwarf accretes hydrogen-rich matter (green region) from a companion. (b) The temperature increases at the base of the envelope until a thermonuclear runaway (TNR) occurs; during the TNR, mixing and diffusion take place at the interface of accreted and white dwarf outer core matter (red region); the convective envelope (orange region) extends almost to the surface. (c) Part of the nuclearly processed matter is ejected (green region) and part settles on the white dwarf (light grey region).

many classical nova light curves show a rapid decline in the optical flux because of extinction, and a corresponding rise in the mid-infrared luminosity because of thermal emission (Shore 2012; Evans & Gehrz 2012). This observation strongly suggests that dust grains, with radii up to ≈ 10 μm (Gehrz et al. 1998; Gehrz 2008), form in the ejecta when they cool to temperatures below ≈ 1700 K. Dust condensation is more common in CO novae and much reduced in ONe novae (Evans & Gehrz 2012). When dust forms, its observed mass fraction in the ejecta is about $\approx 10^{-3}$, corresponding to $\approx 10^{-7} - 10^{-6}$ $M_\odot$ (Bode et al. 1987).

Unlike most other sources, classical novae have been observed to produce carbon-rich and oxygen-rich dust simultaneously (Gehrz 1992). In principle, the composition of the dust that forms in a given environment depends sensitively on the carbon-to-oxygen ratio. When the value of C/O exceeds unity by number, and all oxygen atoms are locked up in strongly bound CO molecules, carbon-rich dust forms; similarly, oxygen-rich dust forms when the value of C/O is less than unity (Waters 2004). This assumes that the carbon monoxide abundance reaches its saturation value. However, if carbon monoxide does not form to saturation, neither carbon nor oxygen will be entirely bound in CO molecules, leaving both elements available for dust condensation (Evans & Rawlings 2008). In addition, José et al. (2004) found that the presence of significant amounts of intermediate-mass elements, such as Al, Ca, Mg, or Si, may dramatically alter the condensation process, allowing for the formation of carbon-rich dust even in a marginally oxygen-rich environment. Table 1 summarizes the measured carbon and oxygen abundances (by mass) in CO nova shells, together with the observation of dust species.

A classical nova is not an ideal environment for dust condensation. Diatomic and polyatomic molecules can only form in the ejecta if they are shielded from ionization by the copious UV radiation of the white dwarf, which remains a supersoft X-ray source for years after the outburst (Schwarz et al. 2011). The shielding can be provided only by spatially inhomogeneous regions of the ejecta that have a much higher than average gas density. Clumpy ejecta have been inferred spectroscopically for several classical novae (Williams 1992; Saizar & Ferland 1994), but their physical origin remains an open question.

The above discussion implies that measuring the isotopic signatures of presolar grains originating from classical novae will shed light on the explosion mechanism, the mixing of matter during the outburst, and the formation of molecules and dust in the expanding ejecta. While several authors have claimed a nova paternity for certain presolar grains, no grains from novae have been unambiguously identified yet. Therefore, they are referred to in the literature as "nova candidate" or "putative nova" grains.

A significant problem is that most classical nova simulations result in ejecta with much more anomalous isotopic ratios compared to what has been measured in the grains (Nittler & Hoppe 2005; Gyngard et al. 2010; Leitner et al. 2012; Nguyen & Messenger 2014). To explain the measurements, it has been speculated (Amari et al. 2001) that these grains may have condensed after the nova ejecta mixed with a much larger amount ($\gtrsim 90\%$) of close-to-solar matter. However, the origin of the latter contribution is not well understood. In addition, counter-arguments favor a supernova origin for some of these "nova candidate" grains (Nittler & Hoppe 2005). Recently, the "first plausible grain of CO nova origin" has been reported, based on the measured C, N, Si, and S isotopic compositions, without requiring any mixing with solar-like matter (Haenecour et al. 2016). This would imply that dust from classical novae contributed to the building blocks of the solar system. A severe problem with this interpretation is the mismatch of the simulated and measured $^{16}O/^{17}O$ and $^{16}O/^{18}O$ ratios in that particular presolar grain, with the deviations amounting to several orders of magnitude.

The total amount of matter ejected by classical novae per year in our galaxy is much smaller compared to the contributions of AGB stars or type II supernovae **(Jordi - please quantify and provide references)**. Nevertheless, it is puzzling that among several thousand presolar grains identified so far, we cannot claim with confidence a classical nova paternity for a single grain. A major problem is that hydrodynamic nova simulations have a poorly constrained parameter space, and that these CPU-expensive simulations sample a restrictive number of parameter combinations only before the computed isotopic ratios are compared with presolar grain measurements. Here, we follow a different approach that explores a large region of the nova parameter space. Since we need to perform a large number of simulations, our method does not rely on a specific classical nova hydrodynamic model, but is by necessity model independent.

Since CO novae are prolific dust producers compared to ONe novae, we will focus in this work on the former objects and leave an investigation of the latter objects to future work. In Section 2, we present our overall strategy. Section 3 discusses our simulation procedure, together with various parameters entering the calculations. Results are presented in Section 4. A summary and conclusions are given in Section 5.

2. Strategy

The two questions we attempt to answer are: (1) Does a given presolar grain originate from a classical nova? (2) What are the conditions that gave rise to the measured isotopic ratios? These questions are intricately connected. If we cannot identify any viable nova conditions that could give rise to the data, we may not claim that a given presolar grain has a nova paternity. These questions have been partially addressed using one-dimensional hydrodynamic nova simulations (José et al. 2004). As with any stellar model, such simulations depend on many assumptions and parameters. Some model parameters are constrained by observation or experiment (e.g., the rate of mass accretion from the companion, thermonuclear reaction rates, and the nuclear energy release), while only indirect information is available for other parameters (e.g., the initial composition of the fuel, initial luminosity and mass of the white dwarf, the amount of white dwarf matter dredged up into the accreted envelope, and the effects of multicycle nova evolution). Some effects have remained nearly unexplored, e.g., the impact of a magnetic field or rotation on the nova outburst. The simulation of dust formation introduces a host of additional assumptions, e.g., the shielding of molecules from the radiation of the white dwarf, the formation of clumpy ejecta, mixing of the ejecta with matter of the interstellar medium or the accretion disk, and grain nucleation and growth to macroscopic size. The main disadvantage of studying the nova paternity of presolar grains with a hydrodynamic model is that only a relatively small number of simulations can be performed. Since the nova parameter space is only sparsely explored, parameter value combinations favorable for reproducing isotopic signatures of nova grains may easily be missed.

We are seeking a more comprehensive exploration of the nova parameter space. To this end, our strategy involves three key ingedients: (i) a simple and fast simulation that can be repeated many times using different combinations of parameter values; (ii) the assumption of a reasonable parameter range and the independent sampling of all parameters; and (iii) the comparison of simulated and observed isotopic ratios for *all* elements measured in a given presolar grain. The latter point is important: the grains condensed at a given time and location in the expanding ejecta. Unless we can explain all of the measured isotopic signatures simultaneously, we may not claim a nova paternity.

In the following, we will discuss each of these ingredients. We start with a description of a schematic model, then add realistic assumptions pertaining to nova outbursts, and finally discuss how to compare our simulation results to presolar grain data.

3. Procedures

3.1. Nuclear reaction network and thermonuclear rates

We compute the nucleosynthesis using a reaction network consisting of 213 nuclides, ranging from p, n, ^{4}He, to ^{55}Cr, that are linked by 2373 nuclear interactions (proton and α-particle captures, β-decays, light-particle reactions, etc.). Thermonuclear reaction rates are adopted from STARLIB v6.1 (11/2016)[1]. This library has a tabular format and contains reaction rates and rate probability density functions on a grid of temperatures between 10 MK and 10 GK (Sallaska et al. 2013). The probability densities can be used to derive statistically meaningful reaction rate uncertainties at any desired temperature. Many of the reaction rates important for the present work that are listed in STARLIB have been computed using a Monte Carlo method, which randomly samples all experimental nuclear physics input parameters (Longland et al. 2010). For some reactions of interest to classical novae (Iliadis 2015), experimental rates are not available yet, and the rates included in STARLIB are adopted from nuclear statistical model calculations using the code TALYS (Goriely et al. 2008). In such cases, a reaction rate uncertainty factor of 10 is assumed. Most of the important reaction rates for studying hydrogen burning in CO novae

[1] Available at: `http://starlib.physics.unc.edu/index.html`.

are based on experimental nuclear physics information and provide a reliable foundation for robust predictions.

Stellar weak interaction rates, which depend on both temperature and density, for all species in our network are adopted from Oda et al. (1994) and, if not listed there, from Fuller, Fowler & Newman (1982). The stellar weak decay constants are tabulated at temperatures from $T = 10$ MK to 30 GK, and densities of $\rho Y_e = 10 - 10^{11}$ g/cm^3, where Y_e denotes the electron mole fraction. For all stellar weak interaction rates, we assumed a factor of 2 uncertainty. Short-lived nuclides, e.g., ^{13}N ($T_{1/2} = 10$ min), ^{14}O ($T_{1/2} = 71$ s), ^{15}O ($T_{1/2} = 122$ s), ^{17}F ($T_{1/2} = 64$ s), and ^{18}F ($T_{1/2} = 110$ min), present at the end of a network calculation were assumed to decay to their stable daughter nuclides.

To explore the effects of thermonuclear reaction rate uncertainties, we will perform some of our calculations by randomly sampling all rates simultaneously using the rate probability densities provided by STARLIB. This method is discussed in detail in Iliadis et al. (2015) and was recently applied to explain abundance anomalies in globular clusters (Iliadis et al. 2016). It suffices to mention here that we adopt a lognormal distribution for the nuclear rates, according to

$$f(x) = \frac{1}{\sigma\sqrt{2\pi}}\frac{1}{x}e^{-(\ln x - \mu)^2/(2\sigma^2)} \qquad (1)$$

where the lognormal parameters μ and σ determine the location and the width, respectively, of the distribution. For a lognormal probability density, samples, i, of a nuclear rate, y, are computed from

$$y_i = y_{med}(f.u.)^{p_i} \qquad (2)$$

where y_{med} and $f.u.$ are the median value and the factor uncertainty, respectively, which are both provided by STARLIB. The quantity p_i is a random variable that is normally distributed, i.e., according to a Gaussian distribution with an expectation value of zero and a standard deviation of unity. We emphasize that the factor uncertainty of experimental Monte Carlo reaction rates depends explicitly on stellar temperature (Iliadis et al. 2010; Longland 2012).

3.2. A schematic model of explosive hydrogen burning

We will adopt a simple, one-zone analytical parameterization for the thermodynamic trajectories of the explosion,

$$T(t) = T_{peak}e^{-t/\tau_T}\ ,\ \rho(t) = \rho_{peak}e^{-t/\tau_\rho} \quad (3)$$

where $t \geq 0$ is the time since peak temperature, T_{peak}, or peak density, ρ_{peak}, and τ_T and τ_ρ are the times at which temperature and density, respectively, have fallen to $1/e$ of their peak values. Notice that we do not assume an adiabatic expansion since we treat τ_T and τ_ρ as independent parameters. This is consistent with the results of one-dimensional hydrodynamic nova simulations, which predict non-adiabatic $T - \rho$ evolutions.

It is imperative to demonstrate that our simple simulation has some predictive power as regards to nova nucleosynthesis. In a first step, we generated a hydrodynamic CO nova model using the one-dimensional code SHIVA (José & Hernanz 1998), assuming a white dwarf mass and initial luminosity of $M_{WD} = 1.0\ M_\odot$ and $L_{WD} = 10^{-2}\ L_\odot$, respectively, and accretion of solar-like material at a rate of $\dot{M}_{acc} = 2 \times 10^{-10}\ M_\odot$ yr^{-1}. The composition of the nuclear fuel was obtained by pre-mixing solar-like matter with carbon-oxygen white dwarf matter (assumed to be 50% ^{12}C and 50% ^{16}O, by mass) with equal amounts. The model included 45 envelope zones containing all material involved in the thermonuclear runaway. The deepest zone achieved a peak temperature of 179 MK, while the innermost ejected zone reached a peak temperature of 163 MK. Final isotopic abundances for matter that exceeds escape velocity (i.e., the fraction of the envelope ejected) are determined 1 hr after peak temperature is achieved, and the abundance of each nuclide is mass-averaged over all ejected zones.

In a second step, we adjusted the parameters of our simple one-zone simulation to see if we can approximately reproduce the final isotopic ratios of the multi-zone hydrodynamic model, assuming exactly the same initial abundances in both calculations. The resulting isotopic ratios for the most important elements (C, N, O, Si, and S) are shown in Figure 2. The solid lines correspond to the time evolutions predicted by the simple one-zone simulation and were obtained with the following parameter values: T_{peak} = 177 MK, ρ_{peak} = 200 g/cm^3, τ_T = 2500 s, τ_ρ = 38 s. The total time was 10,000 s, but the results are not sensitive to this parameter once peak temperature and density have significantly declined from their peak values. The dotted line in each panel indicates the mass-zone-averaged ejected final abundance ratios predicted by the multi-zone hydrodynamic model. The interesting finding is that the one-zone analytic simulation reproduces the results of the multi-zone hydrodynamic calculation *within a factor of 2*. We repeated the test for other CO white dwarf masses, and even for models of ONe novae, and again obtained agreement within a factor of 2.

This level of agreement may be at first surprising, considering that the analytic simulation, unlike the hydrodynamic model, follows a single zone only, and disregards accretion, convection, and ejection of matter. However, recall that we are mainly interested in isotopic *ratios* instead of absolute isotopic or elemental abundances, which are very likely more sensitive to such effects. We emphasize that the parameters derived from the simple simulation (T_{peak}, ρ_{peak}, τ_T, τ_ρ) correspond neither to the averages over different mass zones, nor to a given zone, of the hydrodynamic model. They nevertheless provide, albeit crude, approximations of the physical conditions during the nuclear burning, mainly because thermonuclear reaction rates are highly sensitive to the plasma temperature.

It is also interesting to note that the value ρ_{peak} = 200 g/cm^3 of the exponentially decaying density profile in Figure 2 does not correspond to any maximum density in the one-dimensional hydrodynamic model, but is approximately equal to the *density at maximum temperature* in the innermost zones of the hydrodynamic model. In the latter model, the density declines from a maximum value, typically a few thousand gram per cubic centimeter and achieved well before the temperature peaks, to a very small value.

A factor of two agreement is sufficient for the purposes of the present work, as will be shown below. The advantage of our simple procedure is that we can independently sample over the parameters and repeat the simulation many times. If a given presolar grain has indeed a nova paternity, we would expect that certain combinations of parameter values, T_{peak}, ρ_{peak}, τ_T, τ_ρ, approximately reproduce the measured isotopic ratios, with magnitudes near the ranges typical for classical novae.

Before we can discuss the presolar grain data, however, we need to introduce three more parameters that will be important for our study: the ^{12}C/^{16}O ratio of the outer white dwarf core, the mixing of matter at the interface of the white dwarf and the envelope, and the dilution of the ejecta by mixing with solar-like matter.

3.3. Key parameters for nova nucleosynthesis

3.3.1. The white dwarf composition

Stars with masses between $\approx 0.8 - 8$ M$_\odot$ undergo hydrogen and helium burning in their cores and end their lives as white dwarfs (Karakas & Lattanzio 2014), composed of carbon and oxygen (CO white dwarfs). The composition of the white dwarf depends sensitively on the ^{12}C(α,γ)^{16}O reaction rate. Most

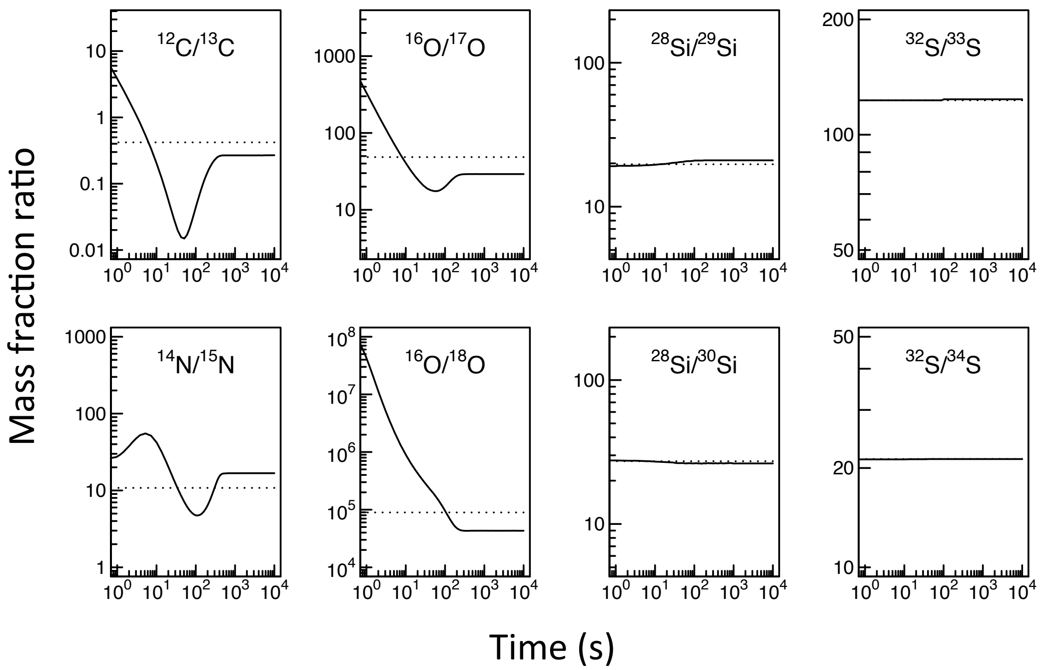

Fig. 2.— Time evolution of C, N, O, Si, and S isotopic ratios as predicted by a parametric, one-zone simulation (solid lines), assuming exponentially decaying temperature and density trajectories. The simulation parameters were T_{peak} = 177 MK, ρ_{peak} = 200 g/cm^3, τ_T = 2500 s, τ_ρ = 38 s. Initial abundances were obtained by pre-mixing solar-like matter with carbon-oxygen white dwarf matter (assumed to be 50% ^{12}C and 50% ^{16}O, by mass) with equal amounts. The dotted lines show the final, mass-zone-averaged results of a one-dimensional hydrodynamic simulation using the same initial composition, where the deepest zone reaching a peak temperature of 179 MK during the outburst.

CO nova studies assume a white dwarf core composition of 50% ^{12}C and 50% ^{16}O, by mass. A rare exception is the work of Kovetz & Prialnik (1997), who performed nova simulations for core compositions of pure ^{12}C, pure ^{16}O, and an equal mixture of ^{12}C and ^{16}O. However, what is most relevant for nova simulations is the composition of the outermost core of the white dwarf, since only this layer is expected to be dredged up during the outburst. Recently, José et al. (2016) evolved an 8 $M_\odot$ progenitor star through successive hydrogen burning, helium burning, and thermally pulsing asymptotic giant branch phases, and used the resulting outer core composition at several locations of the nascent white dwarf as starting points of the CO nova simulations. This resulted in carbon-rich ejecta and the posibility of the formation of carbon-rich dust.

One problem with this assumption is that the white dwarf needs some time to cool before a nova outburst can take place; if the white dwarf is initially too luminous, the envelope is not highly degenerate and only a mild thermonuclear runaway with no mass ejection will occur. For this reason, almost all nova simulations have been performed with an initial white dwarf luminosity in the range of $L_{WD} = 10^{-3} - 10^{-2}$ $M_\odot$. For a few studies assuming higher luminosities, see Starrfield, Sparks, & Truran (1985); Yaron et al. (2005); Hernanz & José (2008). The important point is that the composition of the outer core changes while the white dwarf evolves on its cooling track. This question was studied by Bravo et al. (2011) in connection with models for thermonuclear supernovae. The outer core composition of their 1 $M_\odot$ model white dwarf changed from a ^{12}C/^{16}O mass fraction ratio of 1.8 at the beginning of the cooling track, to 7.2 at the end of core crystallization (see their Figure 1). These compositions are vastly different than the mass fraction ratio of ^{12}C/^{16}O = 1 that is commonly assumed in studies of CO novae.

We do not know the actual ^{12}C/^{16}O mass fraction ratio in the outer white dwarf core that gave rise to the isotopic signatures in a given nova presolar grain. Therefore, we will randomly sample this parameter over the range predicted by white dwarf models ($1.5 \leq {}^{12}\mathrm{C}/{}^{16}\mathrm{O} \leq 8.0$) to see which values, if any, reproduce the presolar grain data.

Another problem with assuming an outer core composition of equal ^{12}C and ^{16}O abundances is that classical novae are expected to recur on time scales of $\approx 10^4 - 10^5$ yr. Each nova outburst leaves behind a remnant hydrogen and helium layer on top of the outer white dwarf core (light grey area in Figure 1a and c). Since this layer takes part in the burning during the next flash (Fujimoto & Iben 1992; Prialnik & Livio 1995), it impacts the composition of the nuclear fuel.

3.3.2. Mixing between white dwarf and accreted matter during the flash

Spectroscopic observations show that CNO elements are considerably enriched relative to hydrogen in many nova ejecta (Gehrz et al. 1998). This enrichment plays a critical role for the dynamic ejection of a portion of the envelope and presumably results from mixing of the outer core white dwarf matter with the accreted matter (red region in Figure 1b). Several mixing mechanisms have been proposed previously, but all face difficulties when confronted with observations (Livio & Truran 1990). However, recent two- and three-dimensional simulations yielded encouraging results by demonstrating that Kelvin-Helmholtz instabilities could lead to an enrichment of the accreted envelope with material from the underlying white dwarf at levels that approximately agree with observations (Casanova et al. 2011, 2016). **(Jordi - please provide relevant Glasner reference)**

So far, multi-dimensional nova simulations incorporate very small nuclear reaction networks ($\approx$ 30 nuclides only), and are not suitable for studying the nucleosynthesis in detail. Consequently, one-dimensional simulations are indispensible for this purpose, but cannot account self-consistently for the mixing at the interface between the outer white dwarf core and the accreted matter. Most one-dimensional simulations work around this problem by artificially "pre-enriching" the envelope with outer core matter to a predetermined degree. The enriched matter is then accreted and its history is followed through the nuclear burning and mass ejection stages.

Frequently, one-dimensional nova simulations assume that the accreted matter from the companion and the white dwarf core material pre-mix with equal mass fractions. Recent work, albeit in the context of ONe novae, hinted at a pre-mixing fraction of 25% white dwarf matter and 75% accreted matter (Kelly et al. 2013), which provides a significantly better fit to the measured abundances in several, but not all, nova ejecta.

While these are encouraging first steps, we are far from being able to predict the degree of element mixing in a given observed nova. In particular, the pre-mixing parameter, f_{pre}, is poorly constrained at present. It is defined by mixing one part of outer white dwarf core matter with f_{pre} parts of accreted solar-like matter,

$$X_{pre} \equiv \frac{X_{WD} + f_{pre} X_{acc}}{1 + f_{pre}} \tag{4}$$

where X_i denotes mass fraction. We will randomly sample this parameter over a reasonable range ($0.5 \leq f_{pre} \leq 5.0$) to see which values best reproduce the presolar grain data. The outer bounds of this interval correspond to white dwarf admixtures of 67% and 17%, respectively.

3.3.3. Dilution of the ejecta

We already mentioned that classical nova simulations result in much more anomalous isotopic ratios compared to the values measured in nova candidate grains. To explain the observations, an additional mixing episode, after the outburst, has been postulated (which we will term "post-mixing"), whereby the ejecta processed by nuclear burning mix with more than ten times the amount of unprocessed, solar-like matter before grain condensation (Amari et al. 2001). The source and mechanism of this potential dilution is not well understood. It is likely that some fraction of the ejecta will first collide with the accretion disk and then later with the companion (Figueira et al. 2017). However, other parts of the ejecta are not expected to undergo any collisions. At present, we neither know the source of the solar-like matter, nor if any post-mixing took place at all.

Since the post-mixing process is poorly constrained at present, our simulations will account for it using a post-mixing parameter, f_{post}, defined by

$$X_{post} \equiv \frac{X_{proc} + f_{post} X_{pris}}{1 + f_{post}} \tag{5}$$

where X_{proc} and X_{pris} denote the mass fractions from the reaction network output (i.e., processed matter) and the pristine matter (i.e., solar-like), respectively. We will sample this parameter over a range of $0 \leq f_{post} \leq 10^4$ to see which values best reproduce the presolar grain data.

3.4. Comparison of simulations to presolar grain data

Isotopic data for all presolar grains that have been suggested over the years to originate from novae are compiled in Table 2. The data are separated according to grain chemistry (SiC, silicate, graphite, and oxide). As already noted above, we have no unambiguous evidence linking any of these grains to a nova paternity. Neither can we exclude unambiguously a nova paternity for many other grains among the thousands of presolar samples measured so far. Our goal is to investigate the conditions, if any, that could give rise to the measured isotopic anomalies.

The values listed for C, N, and O represent isotopic number abundance ratios, while for Mg, Si, and S the data correspond to parts-per-thousand deviations from solar matter, e.g.,

$$\begin{aligned} &\delta\left({}^{25}\mathrm{Mg}/{}^{24}\mathrm{Mg}\right) \equiv \delta^{25}\mathrm{Mg} \\ &\equiv \left[\frac{\left({}^{25}\mathrm{Mg}/{}^{24}\mathrm{Mg}\right)_{exp}}{\left({}^{25}\mathrm{Mg}/{}^{24}\mathrm{Mg}\right)_{\odot}} - 1\right] \times 1000 \end{aligned} \tag{6}$$

where the most abundant isotope of the element (i.e., of even mass number) appears in the denominator. We omitted from the table values for δ^{26}Mg that have been reported for some of the grains. Grains condense in nova ejecta about a month after the outburst, but the half-life of ^{26}Al is $\mathrm{T}_{1/2} = 717,000$ yr. We cannot reliably compare the simulated and measured δ^{26}Mg values because some of the observed ^{26}Mg may have condensed originally as ^{26}Al. Neither can we add the simulated ^{26}Mg and ^{26}Al abundances and compare the total to the measured δ^{26}Mg values because aluminum and magnesium may have condensed in a particular grain with different efficiencies. We also omitted any inferred ^{26}Al/^{27}Al ratios. These were obtained from whole-grain measurements, assuming a solar ^{26}Mg/^{24}Mg ratio at the time of grain condensation, which may be a questionable assumption. **(Larry - please edit; might mention here that more reliable results could be obtained if "isochrons" can be constructed for a single grain; but I don't think that was the case for the grains that we list; also, there is a possibility for Al contamination...)**

When comparing grain measurements to results from nucleosynthesis simulations, two important issues need to be addressed. First, we cannot reasonably expect that a simulation will precisely reproduce the grain measurements, since there are too many approximations involved in any stellar model. If the simulation results are "close" to the data, say, within some factor, we may accept the computed results as a possible solution. Second, we need to account for the systematic bias in the grain measurements, in addition to the statistical uncertainty that is included in the reported error. Systematic effects arise from contamination, e.g., from sampling the meteorite material surrounding the grain, or from sample preparation. It is important to emphasize that this bias could move a data point into the direction of less anomalous values only, i.e., contamination will not make a grain appear more anomalous than it really is.

We will adopt the following procedure for determining approximate agreement between simulation and measurement ("acceptable solutions"). A simulated abundance ratio is divided and multiplied by a systematic uncertainty factor, n_{sim}, which defines a range for the ratio. This range is then transformed into a range of simulated δ-values, $\delta^A X_{sim}$,

$$\delta^A X_{sim}^{low} \le \delta^A X_{sim} \le \delta^A X_{sim}^{high} \tag{7}$$

Next, using an experimental uncertainty factor, n_{exp}, we define a range around the experimental mean δ-value, $\delta^A X_{exp}^{mean}$, as

$$\begin{aligned} &n_{exp}^{(1-\pi)/2} \times \delta^A X_{exp}^{mean} - n_{exp} \times \delta^A X_{exp}^{err} \\ &\le \delta^A X_{exp}^{mean} \\ &\le n_{exp}^{(1+\pi)/2} \times \delta^A X_{exp}^{mean} + n_{exp} \times \delta^A X_{exp}^{err} \end{aligned} \tag{8}$$

where $\pi = sign(\delta^A X_{exp}^{mean}) = \pm 1$ denotes the sign of the experimental mean value. We define an acceptable solution if the two regions given by Equations 7 and 8 overlap. For the two factors containing the effects of the simulation and measurement bias, we adopt values of $n_{sim} = 3$ and $n_{exp} = 2$. The former value is chosen to be larger than a factor of 2, within which our one-zone analytic simulations reproduce the results of the multi-zone hydrodynamic calculation (Section 3.2). As already pointed out in Section 2, we will only accept solutions for which simulated and measured δ-values overlap for *all measured isotopic ratios*.

4. Results

We will first show what results can be obtained with our method by using grain LAP-149 as an example. We then summarize results for all nova candidate grains. Finally we discuss those grains that most likely originate from CO novae.

4.1. Example: grain LAP-149

The nova candidate graphite grain LAP-149 has a diameter of about 1 μm and exhibits one of the lowest $^{12}C/^{13}C$ ratios ever measured (Table 2). The $^{14}N/^{15}N$ ratio is high, but the oxygen, silicon, and sulfur isotopic ratios are close to solar within experimental uncertainties. Haenecour et al. (2016) found that the C, N, Si, and S isotopic ratios could be reproduced by a CO nova model involving a 0.6 $M_\odot$ white dwarf with 50% premixing ($f_{pre} = 1$; Equation 4) without assuming any post-mixing. However, the measured and simulated $^{17}O/^{16}O$ and $^{18}O/^{16}O$ ratios disagreed by orders of magnitude. The other CO nova models, for white dwarf masses in the range of $M_{WD} = 0.8 - 1.15\ M_\odot$, did not provide a match to any of the measured isotopic ratios. Notice that LAP-149 is the only nova candidate grain with eight different measured isotopic ratios (see Table 2).

Our results for LAP-149 are shown in Figure 3, which was obtained after computing 25,000 network samples. The top row displays the measured isotopic ratios (red) together with the simulations. Only those simulation results are displayed that simultaneously agree with all data, according to Equations 7 and 8. The different colors for the simulation results correspond to different peak temperature values (black: $T_{peak} \leq 0.15$ GK; blue: 0.15 GK $< T_{peak} <$ 0.20 GK, green: $T_{peak} \geq$ 0.20 GK). The corresponding sampled model parameters are shown in the bottom row.

We obtain acceptable solutions for a wide range of pre-mixing fractions, between f_{pre} = 1 and f_{pre} = 5 (first bottom panel), corresponding to outer white dwarf core admixtures between 50% and 16%, respectively. Post-mixing fractions are in the range of f_{post} = 30 − 100, implying a significant admixture of solar-like matter after the explosion. In particular, no acceptable solutions are obtained without post-mixing, in agreement with the findings of Haenecour et al. (2016). Acceptable peak temperature and peak density values (second bottom panel) scatter throughout the sampled ranges (150 MK $\leq T_{peak} \leq$ 250 MK, 5 g/cm$^3 \leq \rho_{peak} \leq 5 \times 10^3$ g/cm^3). The 1/e exponential decay times for temperature and density (third bottom panel) scatter within the range of 10^3 s $\leq \tau_T \leq 10^4$ s and 10^2 s $\leq \tau_\rho \leq 10^4$ s, respectively. Solutions are obtained for the entire range of sampled outer white dwarf core composition, $0.6 \leq X_{WD}(^{12}C) \leq 0.9$, $0.1 \leq X_{WD}(^{16}O) \leq 0.4$ (fourth bottom panel). Lastly, the ratios of elemental carbon to oxygen, after post-mixing, are in the range of X(C)/X(O) = 0.6 − 1.0 (fifth bottom panel).

So far, we used in the simulations for all rates of thermonuclear reactions and weak interactions their recommended (i.e., median) values provided by STARLIB (Section 3). However, the nuclear rates have uncertainties, either derived from experimental nuclear physics input or from theoretical models (Section 3.1). For this reason, we repeated the above Monte Carlo procedure of computing 25,000 network samples, but this time including the random sampling of the nuclear rates according to their probability densities contained in STARLIB (Section 3). As a result, the scatter of the simulation points (black, blue, green) in Figure 3 increased slightly, but all relevant features discussed above were preserved. In other words, current reaction rate

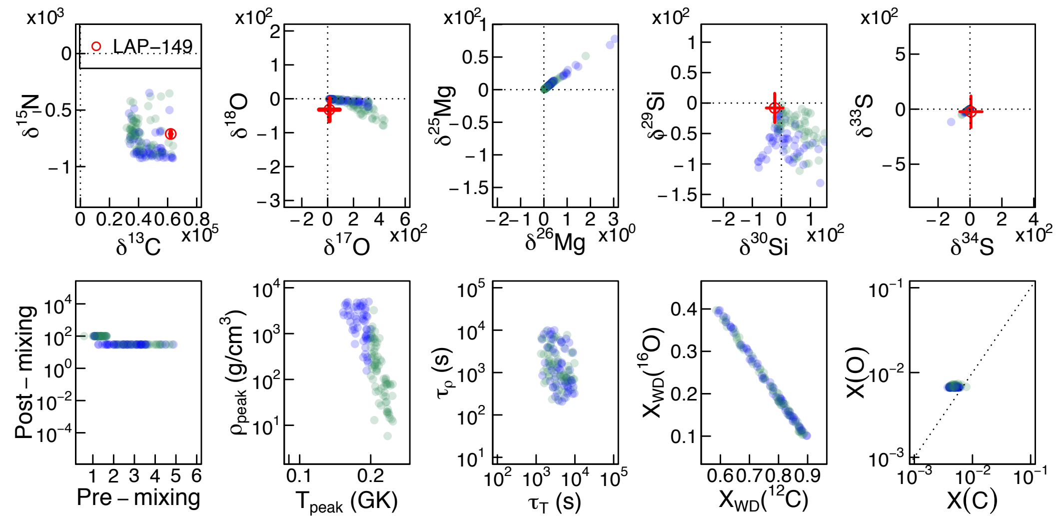

Fig. 3.— Summary results for the presolar graphite grain LAP-149, the only nova candidate grain with eight different measured isotopic ratios. (Top row) Isotopic ratios for C, N, O, Mg, Si, and S. The data points are shown in red; simulations that reproduce all data simultaneously (see Equations 7 and 8) are displayed in black, blue, and green, depending on the sampled peak temperature (see below). (Bottom row) From left to right: post-mixing fraction versus pre-mixing; peak density versus peak temperature; 1/e exponential decay times for the density evolution versus temperature evolution; outer white dwarf mass fractions of ^{16}O versus ^{12}C; and elemental oxygen versus carbon mass fractions *after* post-mixing. The black, blue, and green simulation results correspond to peak temperatures of $T_{peak} \leq 0.15$ GK, 0.15 GK $< T_{peak} < 0.20$ GK, and $T_{peak} \geq 0.20$ GK, respectively. The simulation results were obtained with recommended nuclear interaction rates only, i.e., without Monte Carlo sampling of the nuclear rates.

uncertainties have only a small impact on our results for this particular presolar grain.

The above results do not *prove* a CO nova origin for LAP-149, because we are not considering here the production in sites other than novae. But we can conclude that this grain could have been produced by the temperature and density conditions, and compositions, typical of CO novae. However, the ejecta must have been mixed with a larger fraction of solar-like matter, i.e., 1 part of ejecta with at least 30 parts of solar-like matter.

4.2. Results for all nova candidate grains

Similar to grain LAP-149 discussed in the previous section, we investigated for each of the 39 grains listed in Table 2 if our simulations can reproduce the measured isotopic ratios according to Equations 7 and 8. Three points need to be considered for the following discussion.

First, the number of measured isotopic ratios will strongly impact the likelihood that a given grain originates from a CO nova. In other words, if simulations reproduce to a similar degree the data for grains A and B, and only two isotopic ratios have been measured in grain A compared to 6 ratios in grain B, then the latter grain is more likely to be of CO nova paternity. Clearly, the more isotopic ratios have been measured, the tighter the constraints on the grain origin.

Second, the relative number of network runs ("acceptable solutions") that provide simultaneous solutions for all measured isotopic ratios of a given grain is also important in this regard. We cannot claim that the *absolute* number of acceptable solutions reflects the probability of a CO nova paternity. But we can conclude that a low number of solutions indicates a fine-tuning of model parameters, while a high number of solutions results from model parameter combinations that occupy a larger volume of the parameter space. In other words, the *relative* number of acceptable solutions reflects the likelihood of a CO nova paternity.

Third, we discussed in Section 3.3.3 that the origin and mechanism for a possible dilution of the ejecta by solar-like matter ("post-mixing") is not well understood, and that it is likely that a fraction of CO nova grains condense in the ejecta without any post-mixing. For this reason, we assume that a given grain has a higher chance of a CO nova paternity if its measured isotopic ratios can be simulated without any post-mixing.

If we allow for post-mixing of various degrees, we find acceptable solutions for almost all grains listed in Table 2. The only exceptions are grains 8-9-3 and KFC1a-551. For these, not a single acceptable solution is obtained, and thus a CO nova paternity is very unlikely. Also, it would be a furtuitous coincidence if all of the other 37 presolar grains listed in Table 2 would be of CO nova origin. Therefore, we conclude that only a weak case can be made for a CO nova paternity if post-mixing must be invoked to match observed and simulated isotopic ratios.

Table 3 provides an overview of our results obtained *without assuming any post-mixing.* For each grain we list the mineralogy, the number of measured isotopic ratios, and the measured elements. The last column shows the total number of network runs that provide simultaneous solutions for all measured isotopic ratios of a given grain according to Equations 7 and 8. The grains are rank ordered, from top to bottom, according to the plausibility of a CO nova paternity. As discussed above, we ranked the grains according to the number of measured isotopic ratios (column 3) and the number of acceptable simulations (column 5).

We find that six grains, all of them of the SiC variety, have a high plausibility of a CO nova origin (from G270-2 to Ag2_6 in Table 3). These grains will be discussed in more detail in Section 4.3. In this case, we obtain acceptable solutions without any post-mixing, and we have several measured isotopic ratios (≥4) or many acceptable solutions (≥10).

The next group consists of twelve grains (from Ag2 to 1_07 in Table 3) that do not require any post-mixing. These have a medium plausibility of a CO nova paternity. We rank them below the top group because they either have a small number of measured isotopic ratios (i.e., fewer experimental constraints) or a small number of acceptable simulations.

Figure 4 shows the measured C, N, O, Si, and S isotopic ratios of all grains listed in Table 2. The colors red and green indicate grains of high and medium plausibility, respectively, of a CO nova paternity. For these two groups, acceptable solutions are obtained without assuming any post-mixing of the ejecta. Grains shown in blue require post-mixing to match the measured isotopic ratios and correspond to a low plausibility of a CO nova paternity. For the two grains shown in black, no solutions are obtained with or without post-mixing of the ejecta, and thus they most likely do not originate from CO novae.

4.3. High-plausibility CO nova grains

The SiC grains G270-2, G278, Ag2_6 (Liu et al. 2016), and M11-334-2, M11-347-4, M11-151-4 (Nittler & Hoppe 2005), shown in boldface in Table 3, have the highest plausibility of a CO nova paternity. For these grains, between four and six isotopic ratios of the elements C, N, Si, and S have been measured, and our simulations sampling the CO nova parameter space provide simultaneous solutions to all data without requiring any dilution of the ejecta with solar-like matter.

Larry - please add a paragraph with the characteristics of these grains, if necessary....

We will now consider the simulated peak temperature and peak density conditions that are obtained for these grains, assuming no post-mixing. They are shown in Figure 5, using the same color scheme that was employed in Figure 3 (black, blue, and green for $T_{peak} \leq 0.15$ GK, 0.15 GK $< T_{peak} < 0.20$ GK, and $T_{peak} \geq 0.20$ GK, respectively). The simulation results are not uniformly spread over the $T_{peak} - \rho_{peak}$ plane. Instead, the solutions occupy select regions. Black simulation points are not apparent, except for a small number of points for grains G278 and M11-334-2. This indicates that all six grains likely originate in nova explosions with peak temperatures in excess of 150 MK, involving higher-mass CO white dwarfs. For grains G270_2 and Ag2_6, the most likely peak temperature exceeds 200 MK, as can be seen from the relative number of green simulation points. Figure 6 shows for the same six grains the exponential 1/e decay time scale of the density profile versus the exponential 1/e decay time scale of the temperature profile. The simulation points occupy a parameter space typical for CO nova conditions.

It is interesting to consider the measured elemental carbon and oxygen abundances in CO nova ejecta, and compare the observations to the simulations. The observational results are summarized in Table 1. The carbon-to-oxygen mass fraction ratios are in the range of 0.084 (for GQ Mus) to 5.4 (for V827 Her). Dust has been directly observed in PW Vul, QV Vul, V827 Her, V842 Cen, and V1668 Cyg (column 5). At least two of these, QV Vul and V842 Cen, have produced SiC dust. The simulated elemental oxygen versus carbon abundances (by mass) are shown in Figure 7, without assuming any post-mixing. Most of the simulation results scatter about the dotted line, corresponding to equal carbon and oxygen mass fractions. A few simulation points, for grain G278 only, exhibit ratios of $X(O)/X(C) \lesssim 0.3$ (i.e., the points on the far left in the second top panel), which would be unfavorable for the condensation of SiC grains. For all solutions shown in Figure 7,

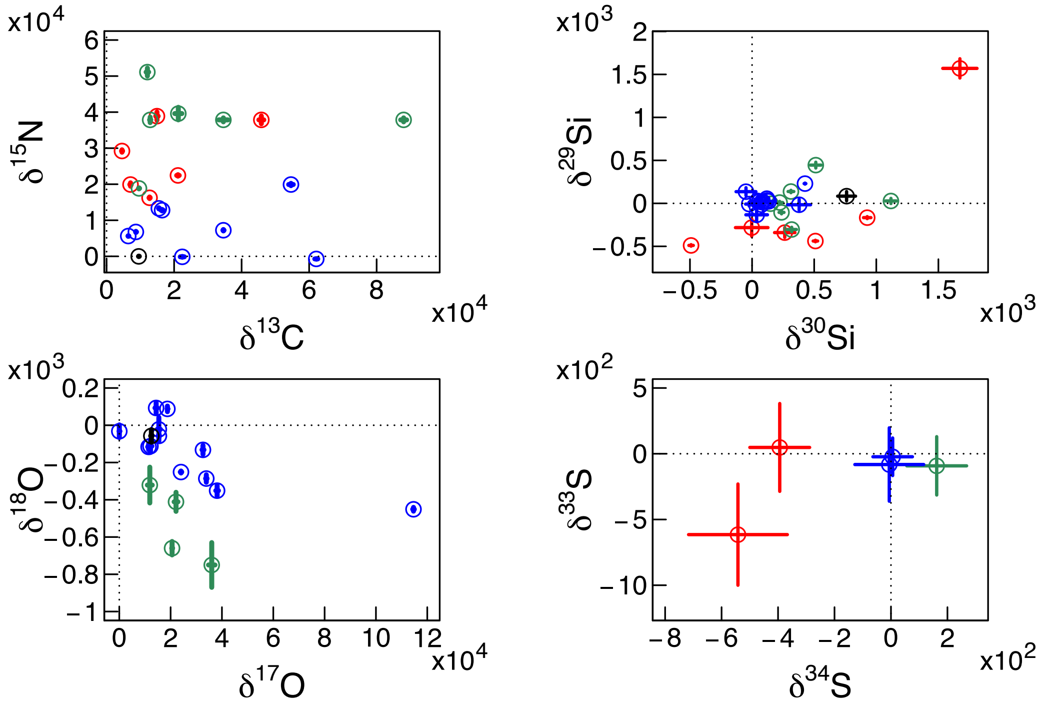

Fig. 4.— Measured isotopic ratios for the elements C, N, Si, and S (see Table 2). The colors red and green indicate grains of high and medium plausibility, respectively, of a CO nova paternity (see discussion in the text); for these two groups, acceptable solutions are obtained without requiring any post-mixing of the ejecta. Grains shown in blue require post-mixing to match the measured isotopic ratios and correspond to a low plausibility of a CO nova paternity. For the two grains shown in black, no solutions are obtained even with post-mixing of the ejecta; thus it is highly unlikely that they originate from CO novae.

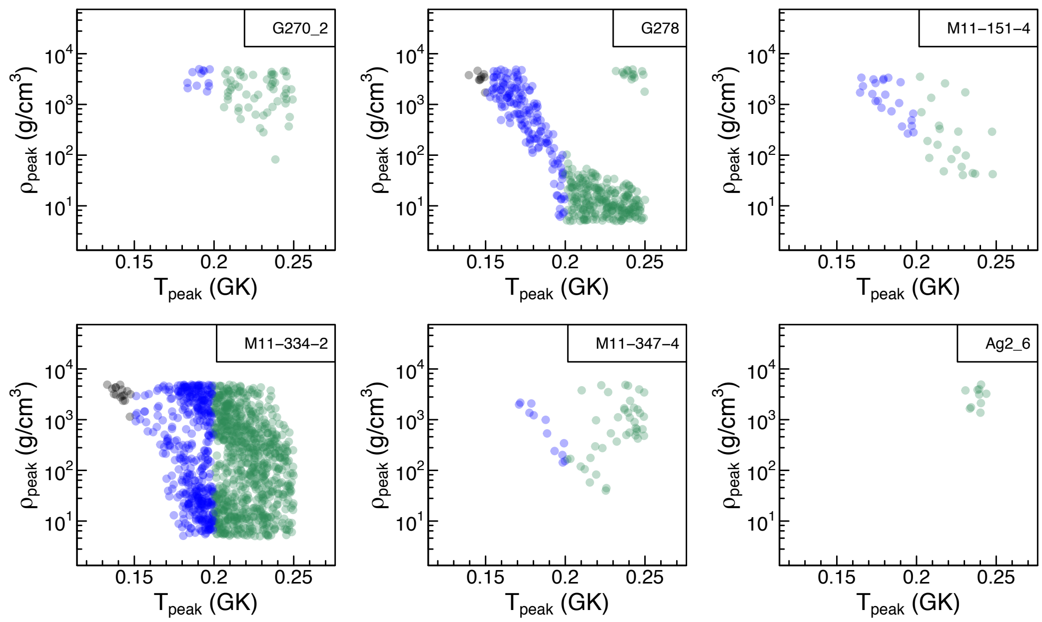

Fig. 5.— Peak density, ρ_{peak}, versus peak temperature, T$_{peak}$, for the six presolar grains with the highest plausibility of a CO nova paternity. These are shown in boldface in column 5 of Table 3. The colors have the same meaning as in Figure 3. The simulation results, using 50,000 network calculations, were obtained assuming no post-mixing of ejecta with solar-like matter (f_{post} = 0) and without any variations of thermonuclear reaction rates.

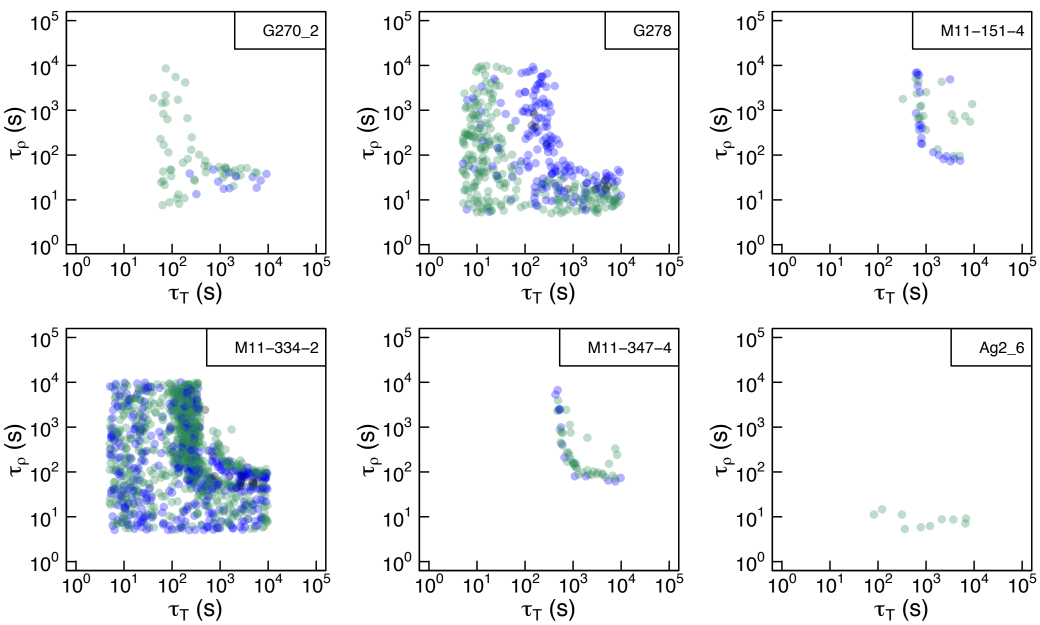

Fig. 6.— Exponential 1/e decay time scale of the density profile versus the exponential 1/e decay time scale of the temperature profile, for the six presolar grains with the highest plausibility of a CO nova paternity (shown in boldface in column 5 of Table 3). The colors have the same meaning as in Figure 3. The simulation results, using 50,000 network calculations, were obtained assuming no post-mixing of ejecta with solar-like matter ($f_{post} = 0$) and without any variations of thermonuclear reaction rates.

the median of the elemental silicon mass fraction amounts to $X_{med}(\mathrm{Si}) \approx 6 \times 10^{-4}$, which is close to the solar value, $X_{\odot}(\mathrm{Si}) \approx 8 \times 10^{-4}$.

5. Summary

xxx.

This work was supported by the U.S. Department of Energy under Contract No. DE-FG02-97ER41041 and by NASA under the Astrophysics Theory Program Grant 14-ATP14-0007.

References

Amari, S., Zinner, E., & Lewis, R.S. 1995, AIP Conference Proceedings, 327, 581

Amari, S., Gao, X., Nittler, L.R., Zinner E., José, J., Hernanz, M., & Lewis, R.S. 2001, ApJ, 551, 1065

Arai, A., et al. 2010, Publ. Astron. Soc. Japan, 62, 1103

Bode, M.F., Roberts, J.A., Whittet, D.C.B., Seaquist, E.R., & Frail, D.A. 1987, Nature, 329, 519

Bose, M., Xuchao, Z., Floss, C., Stadermann, F., & Yangting, L. 2010, Proc. Symp. Nucl. Cosm. XI, 138

Bravo, E., Althaus, L.G., García-Berro, E., & Domínguez, I. 2011, A&A, 526, A26

Casanova, J., José, J., García-Berro, Shore, S.N., & Calder A.C. 2011, Nature, 478, 490

Casanova, J., José, J., García-Berro, & Shore, S.N. 2016, A&A, 595, A28

Chesneau, O., et al. 2008, A&A, 487, 223

Choi, B.-G., Wasserburg, G.J., & Huss, G.R. 1999, ApJ, 522, L133

Evans, A., & Rawlings, J.M.C. 2008, in: Classical Novae, 2nd ed., ed. M.F. Bode and A. Evans (Cambridge University Press: Cambridge)

Evans, A., et al. 2017, MNRAS, 466, 4221

Evans, A., & Gehrz, R.D. 2012, Bulletin of the Astronomical Society of India, 40, 213

Ferland, G.J., & Shields, G.A. 1978, ApJ, 226, 172

Figueira, J., José, J., García-Berro, E., Campbell, S.W., García-Senz, D., & Mohamed, S. 2017, A&A, submitted

Fujimoto, M., & Iben, I. 1992, ApJ, 399, 646

Fuller, G. M., Fowler, W. A., & Newman, M. J. 1982, ApJS, 48, 279

Gehrz, R.D. 1992, ApJ, 400, 671

Gehrz, R.D., Truran, J.W., Williams, R.E., & Starrfield, S. 1998, PASP, 110, 3

Gehrz, R.D. 2008, in: Classical Novae, 2nd ed., ed. M.F. Bode and A. Evans (Cambridge University Press: Cambridge)

Goriely, S., Hilaire, S., & Koning, A.J. 2008, A&A, 487, 767

Gyngard, F., Zinner, E., Nittler, L.R., Morgand, A., Stadermann, F.J., & Hynes, M. 2010, ApJ, 717, 107

Haenecour, P., Floss, C., José, J., Amari, S., Lodders, K., Jadhav, M., Wang, A., & Gyngard, F. 2016, ApJ, 825, 88

Helton, L.A. 2010, PhD thesis, University of Minnesota

Hernanz, M., & José, J. 2008, New Astronomy, 52, 386

Hric. L., Petrík, K., Urbam, Z., & Hanzl, D. 1998, A&A, Supplement Series, 133, 211

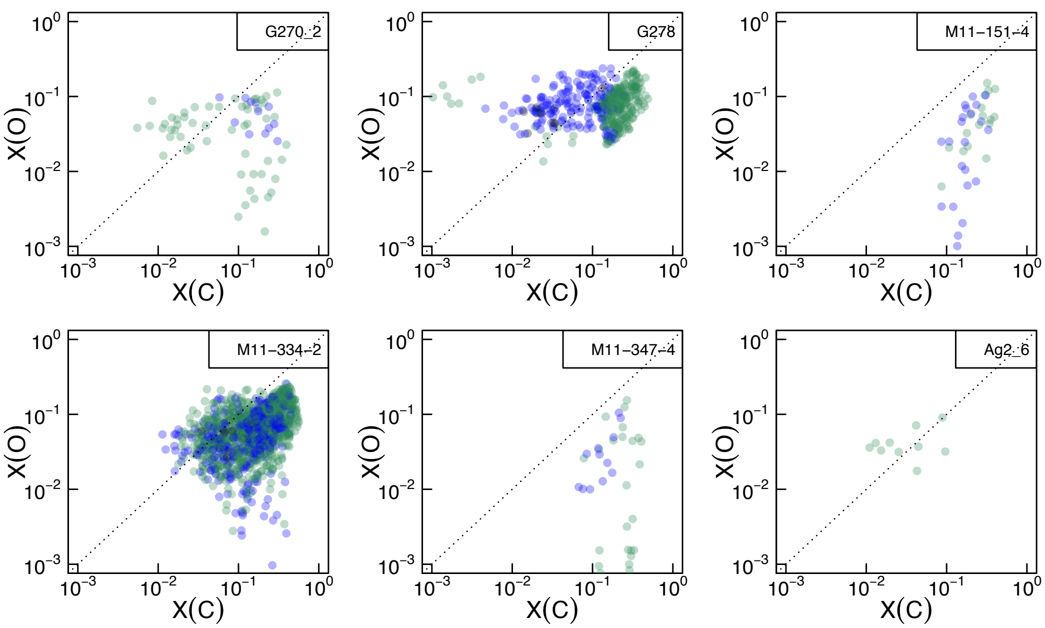

Fig. 7.— Elemental oxygen versus elemental carbon abundance (by mass) in the ejecta, for the six presolar grains with the highest plausibility of a CO nova paternity (shown in boldface in column 5 of Table 3). The colors have the same meaning as in Figure 3. The simulation results, using 50,000 network calculations, were obtained assuming no post-mixing of ejecta with solar-like matter (f_{post} = 0) and without any variations of thermonuclear reaction rates. The dotted lines corresponds to equal mass fractions.

Iliadis, C. 2015, Nuclear Physics of Stars (Wiley-VCH)

Iliadis, C., Longland, R., Champagne, A.E., Coc, A., & Fitzgerald, R. 2010, Nucl. Phys. A, 841, 31

Iliadis, C., et al. 2015, J. Phys. G: Nucl. Part. Phys., 42, 034007

Iliadis, C., Karakas, A.I., Prantzos, N., Lattanzio, J.C., and Doherty, C.L. 2016, ApJ, 818, 98

José, J. 2016, Stellar Explosions. Hydrodynamics and Nucleosynthesis (CRC Press)

José, J., & Hernanz, M. 1998, ApJ, 494, 680

José, J., Hernanz, M., García-Berro, E., & Gil-Pons, P. 2003, ApJ, 597, L41

José, J., Hernanz, M., Amari, S., Lodders, K., & Zinner, E. 2004, ApJ, 612, 414

José, J., & Hernanz, M. 2007, Meteoritics & Planetary Science, 42, 1135

José, J., Halabi, G.M., & El Eid, M. 2016, A&A, 593, A54

Karakas, A.I., & Lattanzio, J.C. 2014, PASA, 31, e030

Kawakita, H., Fujii, M., Nagashima, M., Kajikawa, T., Kubo, N., & Arai, A. 2015, Publ. Astron. Soc. Japan, 67, 17 (1-8)

Kawakita, H., Ootsubo, T., Arai, A., Shinnaka, Y., & Nagashima, M. 2017, AJ, 153, 74

Kelly, K.J., Iliadis, C., Downen, L., José, J., & Champagne, A.E. 2013, ApJ, 777, 130

Kovetz, & Prialnik, D. 1997, ApJ, 477, 356

Leitner, J., Kodolányi, Hoppe, P., & Floss, C. 2012, ApJ, 754, L41

Liu, N., Nittler, L.R., Alexander, C.M.O'D., Wang, J., Pignatari, M., José, J., & Nguyen, A. 2016, ApJ, 820, 140

Livio, M., & Truran, J.W. 1990, Ann. NY Acad. Sci. 617, 126

Longland, R. et al. 2010, Nucl. Phys. A, 841, 1

Longland, R. 2012, A&A, 548, A30

Lyke, J.E., et al. 2001, AJ, 122, 3305

Munari, U., et al. 2008, A&A, 492, 145

Nguyen, A.N., Stadermann, F.J., Zinner, E., Stroud, R., Alexander, C.M.O'D., & Nittler, L.R. 2007, ApJ, 656, 1223

Nguyen, A.N., Nittler, L.R., Stadermann, F.J., Stroud, R., & Alexander, C.M.O'D., & Nittler, L.R. 2010, ApJ, 719, 166

Nguyen, A.N., & Messenger, S. 2014, ApJ, 784, 149

Nittler, L.R., Alexander, C.M.O'D., Gao, X., Walker, R.M., & Zinner, E. 1997, ApJ, 483, 475

Nittler, L.R., & Alexander, C.M.O'D. 2003, Geochim. Cosmochim., 67, 4961

Nittler, L.R., & Hoppe, P. 2005, ApJ, 631, L89

Nittler, L.R., Alexander, C.M.O'D., Gallino, R., Hoppe, P., Nguyen, A.N., Stadermann, F.J., & Zinner, E.K. 2008, ApJ, 686, 1524

Nittler, L. R., & Cielsa, F. 2016, Annu. Rev. Astron. Astrophys., 54, 53

Oda, T. et al. 1994, Atom. Data Nucl. Data Tab., 56, 231

Prialnik, D., & Livio, M. 1995, PASP, 107, 1201

Saizar, P., & Ferland, G.J. 1994, ApJ, 425, 755

Sakon, I., et al. 2016, ApJ, 817, 145

Sallaska, A. et al. 2013, ApJS, 207, 18

Schwarz, G.J. 2002, ApJ, 577, 940

Schwarz, G.J., et al. 2001, MNRAS, 320, 103

Schwarz, G.J., et al. 2007, AJ, 134, 516

Schwarz, G.J., et al. 2011, ApJS, 197, 31

Shore, S.N. 2012, Bulletin of the Astronomical Society of India, 40, 185

Starrfield, S., Sparks, W.M., & Truran, J.W. 1985, ApJ, 291, 136

Starrfield, S., Sparks, W.M., & Truran, J.W. 1986, ApJ, 303, L5

Starrfield, S., Iliadis, C., Hix, W.R., Timmes, F.X., Sparks, W.M. 2009, ApJ, 692, 1532

Starrfield, S., Iliadis, C, & Hix, W.R. 2016, Pub. Astron. Soc. Pacific, 128, 051001

Vollmer, C., Hoppe, P., Brenker, F., & Holzapfel, C. 2007, ApJ, 666, L49

Waters, L.B.F.M. 2004, in: Astronomical Society of the Pacific Conf. Series, Vol. 309, Astrophysics of Dust, eds. A.N. Witt, G.C. Clayton, & B.T. Draine, 229

Williams, R.E. 1992, ApJ, 392, 99

Yaron, O., Prialnik, D., Shara, M.M., & Kovetz, A. 2005, ApJ, 623, 398

Zinner, E. 2014, in: Treatise on Geochemistry, Vol. 1, 2nd ed., ed. A.M. Davis (Elsevier: Oxford), 181

This 2-column preprint was prepared with the AAS LATEX macros v5.2.

Table 1

Carbon, oxygen, and dust in CO novae.[a]

CO nova	X(C)[b]	X(O)[b]	X(C)/X(O)	Type of dust[c]	Mass of dust ($M_\odot$)
GQ Mus	0.0080	0.095	0.084	none detected	···
HR Del	···	0.047	···	···	···
LMC 1991	···	···	0.27[f]	···	···
PW Vul	0.031	0.047	0.66	C	5.1×10^{-10}
QV Vul	···	0.041	···	C, SiO_2, HC, SiC	1.0×10^{-6}[j]
V339 Del	···	···	···	···	5×10^{-9}[m]
V443 Sct	···	0.007	···	···	···
V705 Cas[n]				C, HC, SiO_2	8.2×10^{-7}[j]
V827 Her	0.087	0.016	5.4	C	···
V842 Cen	0.12	0.03	4.0	C, SiC, HC	···
V1186 Sco	···	···	···	none detected[i]	···
V1280 Sco	···	···	···	C, SiO_2[g]	1.0×10^{-7}[l]
V1425 Aql	0.030[d]	0.085[d]	0.35	···	···
V1668 Cyg	···	···	···	C	2.1×10^{8}[j]
V2214 Oph	···	0.060	···	···	···
V2362 Cyg	···	0.163[e]	···	···	$\approx 2\times10^{-10} - 2\times10^{-8}$[k]
V2676 Oph	···	···	···	C, SiO_2[h]	···

[a]From Gehrz et al. (1998), unless noted otherwise; if more than one value is quoted, we adopt the arithmetic average value.

[b]Abundance by mass.

[c]C=amorphous carbon; HC=hydrocarbons; SiO_2=silicate.

[d]From Lyke et al. (2001).

[e]From Munari et al. (2008).

[f]From Schwarz et al. (2001).

[g]From Sakon et al. (2016).

[h]From Kawakita et al. (2017); also reported by Kawakita et al. (2015): $^{12}C/^{13}C \approx 4$ and $^{14}N/^{15}N \approx 2$.

[i]From Schwarz et al. (2007).

[j]From Gehrz (2008).

[k]From Arai et al. (2010).

[l]From Chesneau et al. (2008).

[m]From Evans et al. (2017).

[n]Hric et al. (1998) suggest a white dwarf mass of 0.79 ± 0.06 $M_\odot$.

Table 2

Measured isotopic ratios in nova candidate presolar grains

Grain	$^{12}C/^{13}C$	$^{14}N/^{15}N$	$^{17}O/^{16}O$ ($\times10^{-4}$)	$^{18}O/^{16}O$ ($\times10^{-3}$)	$\delta^{25}Mg/^{24}Mg$	$\delta^{29}Si/^{28}Si$	$\delta^{30}Si/^{28}Si$	$\delta^{33}S/^{32}S$	$\delta^{34}S/^{32}S$
SiC Grains									
AF15bB-429-3[1]	9.4 ± 0.2	...	...	...	...	28 ± 30	1118 ± 44	...	...
AF15bC-126-3[1]	6.8 ± 0.2	5.22 ± 0.11	...	...	...	-105 ± 17	237 ± 20	...	...
Ag2[2]	2.5 ± 0.1	7.0 ± 0.1	...	...	...	-304 ± 26	319 ± 38	-92 ± 222	162 ± 106
Ag2_6[2]	16.0 ± 0.4	9.0 ± 0.1	...	...	...	-340 ± 57	263 ± 82	48 ± 334	-394 ± 106
KJC112[1]	4.0 ± 0.2	6.7 ± 0.3	...	...	...	...	...	...	...
KJGM4C-100-3[1]	5.1 ± 0.1	19.7 ± 0.3	...	...	...	55 ± 5	119 ± 6	...	...
KJGM4C-311-6[1]	8.4 ± 0.1	13.7 ± 0.1	...	...	...	-4 ± 5	149 ± 6	...	...
G1614[2]	9.2 ± 0.07	35.0 ± 0.7	...	...	...	34 ± 5	121 ± 6	...	...
G1697[2]	2.5 ± 0.01	33.0 ± 0.8	...	...	...	-42 ± 12	40 ± 15	...	...
G1748[2]	5.4 ± 0.02	19.0 ± 0.2	...	...	...	21 ± 4	83 ± 5	...	...
G270_2[2]	11.0 ± 0.3	13.0 ± 0.3	...	...	...	-282 ± 101	-3 ± 131	-615 ± 385	-542 ± 175
G283[2]	12.0 ± 0.1	41.0 ± 0.5	...	...	...	-15 ± 3	75 ± 4	...	...
G278[2]	1.90 ± 0.03	7.0 ± 0.2	...	...	...	1570 ± 112	1673 ± 138	...	...
G1342[2]	6.40 ± 0.08	7.00 ± 0.14	...	...	...	445 ± 34	513 ± 43	...	...
GAB[2]	1.60 ± 0.02	13.0 ± 0.2	...	...	...	230 ± 6	426 ± 7	-82 ± 279	-6 ± 122
G240-1[2]	1.00 ± 0.01	7.0 ± 0.1	...	...	...	138 ± 14	313 ± 23	...	...
M11-151-4[3]	4.02 ± 0.07	11.6 ± 0.1	...	...	...	-438 ± 9	510 ± 18	...	...
M11-334-2[3]	6.48 ± 0.08	15.8 ± 0.2	...	...	...	-489 ± 9	-491 ± 18	...	...
M11-347-4[3]	5.59 ± 0.13	6.8 ± 0.2	...	...	...	-166 ± 12	927 ± 30	...	...
M26a-53-8[4]	4.75 ± 0.23	...	...	...	...	10 ± 13	222 ± 25	...	...
Silicate Grains									
1_07[5]	...	...	49.1 ± 3.6	1.36 ± 0.19	...	...	...	...	...
4_2[6]	...	...	128.0 ± 1.4	1.74 ± 0.05	1025 ± 29	24 ± 40	134 ± 52	...	...
4_7[6]	...	...	149.0 ± 2.0	1.30 ± 0.06	213 ± 56	136 ± 46	-49 ± 80	...	...
A094_TS6[7]	...	...	95.4 ± 1.1	1.50 ± 0.01	...	29 ± 43	43 ± 54	...	...
AH-106a[8]	...	...	50.1 ± 2.2	1.78 ± 0.07	...	15 ± 59	80 ± 67	...	...
B2-7[9]	...	...	133.0 ± 1.0	1.43 ± 0.04	...	21 ± 56	57 ± 69	...	...
GR95_13_29[10]	...	...	62.5 ± 2.5	1.96 ± 0.14	79 ± 21	-16 ± 63	379 ± 92	...	...
Graphite Grains									
KFB1a-161[4,11]	3.8 ± 0.1	312 ± 43	...	...	-28 ± 62	-133 ± 81	37 ± 87	...	...
KFC1a-551[4]	8.46 ± 0.04	273 ± 8	...	...	-157 ± 443	84 ± 54	761 ± 72	...	...
LAP-149[12]	1.41 ± 0.01	941 ± 81	3.86 ± 0.34	1.94 ± 0.07	...	-8 ± 24	-23 ± 29	-23 ± 143	6 ± 70
Oxide Grains									
12-20-10[13]	...	...	88.0 ± 3.0	1.18 ± 0.11	...	...	...	...	...
8-9-3[13]	...	...	51.4 ± 1.1	1.89 ± 0.07	-66 ± 21	...	...	...	...
C4-8[13]	...	...	440.4 ±1.2	1.10 ± 0.02	949 ± 8	...	...	...	...
KC23[14]	...	...	58.5 ± 1.8	2.19 ± 0.06	45 ± 35	...	...	...	...
KC33[14]	...	...	82.2 ± 0.6	0.68 ± 0.08	...	...	...	...	...
MCG67[10]	...	...	47.3 ± 1.4	1.77 ± 0.03	...	...	...	...	...
MCG68[10]	...	...	62.6 ±1.1	1.89 ± 0.02	...	...	...	...	...
S-C6087[15]	...	...	75.2 ± 0.3	2.18 ± 0.03	36 ± 22	...	...	...	...
T54[16]	...	...	141 ± 5	0.5 ± 0.2	...	...	...	...	...
Solar	89	272	3.8	2.0	0.0	0.0	0.0	0.0	0.0

Note.—Presented errors are 1σ. Some ratios are presented as deviations from solar abundances in permil, $\delta^{i}X/^{j}X \equiv [(^{i}X/^{j}X)/(^{i}X/^{j}X)_{\odot}-1]\times1000$. $^{12}C/^{13}C$ and $^{14}N/^{15}N$ (ratio in air) are from José et al. (2004) and references therein; $^{17}O/^{16}O$ and $^{18}O/^{16}O$ solar values are from Leitner et al. (2012). Multiple values exist for the $^{16}O/^{18}O$ (or $^{18}O/^{16}O$) ratio of Grain KFC1a-551 and are not given here (see: Amari, Zinner, & Lewis (1995); M. Bose, priv. comm. (2017); and http://presolar. wustl. edu/~pgd.

References. — [1]Amari et al. (2001); [2]Liu et al. (2016); [3]Nittler & Hoppe (2005); [4]Nittler & Alexander (2003); [5]Vollmer et al. (2007); [6]Nguyen & Messenger (2014); [7]Nguyen et al. (2007); [8]Nguyen et al. (2010); [9]Bose et al. (2010); [10]Leitner et al. (2012); [11]José & Hernanz (2007); [12]Haenecour et al. (2016); [13]Gyngard et al. (2010); [14]Nittler et al. (2008); [15]Choi, Wasserburg, & Huss (1999); [16]Nittler et al. (1997).

Table 3

Summary results of our simulations[a] . The order, from top to bottom, reflects approximately the likelihood that a given grain originated from a CO nova.

Grain[b]	Mineralogy[b]	Number of isotopic ratios[c]	Measured elements[c]	Number of solutions[d]
G270-2	SiC	6	C, N, Si, S	67
M11-334-2	SiC	4	C, N, Si	1228
G278	SiC	4	C, N, Si	425
M11-347-4	SiC	4	C, N, Si	56
M11-151-4	SiC	4	C, N, Si	43
Ag2_6	SiC	6	C, N, Si, S	10
Ag2	SiC	6	C, N, Si, S	3
G1342	SiC	4	C, N, Si	11
AF15bC-126-3	SiC	4	C, N, Si	5
G240-1	SiC	4	C, N, Si	8
KJGM4C-311-6	SiC	4	C, N, Si	2
AF15bB-429-3	SiC	3	C, Si	102
M26a-53-8	SiC	3	C, Si	7
T54	oxide	2	O	11048
KC33	oxide	2	O	8840
KJC112	SiC	2	C, N	1315
12_20_10	oxide	2	O	330
1_07	silicate	2	O	3

[a]Results were obtained without post-mixing, i.e., without any dilution of the ejecta before grain condensation.

[b]See Table 2; the grains in boldface have the highest plausibility for a CO nova paternity.

[c]Measured number of isotopic ratios and elements in grain.

[d]The number of network runs, out of a total of 50,000 simulations, that provide simultaneous solutions for all measured isotopic ratios of a given grain.